Research Article / Review Article FUPRE JOURNAL 8(2): 150-171(2024)

FUPRE Journal

of

Scientific and Industrial Research

ISSN: 2579-1184(Print) ISSN: 2578-1129 (Online)

http://fupre.edu.ng/journal

Thermal Analysis of a Serpentine tube Absorber Plate Solar Collector System using Experimental and CFD Simulation

ANIEKAN, E. I. [1,*], *EGHOSA, O.* [2]

[1]Department of Mechanical Engineering, Akwa Ibom State Polytechnic, Ikot Osurua, Nigeria

[2]Department of Mechanical Engineering, University of Benin, Benin City, Nigeria

ARTICLE INFO

Received: 10/09/2023
Accepted: 22/12/2023

Keywords

Absorber plate, Serpentine tube, Simulation, Thermal analysis

ABSTRACT

Solar energy is a promising renewable energy source that can be harnessed through various technologies, including solar collectors. The objective was to evaluate the system's thermal performance and understand the heat transfer mechanisms involved. Experimental analysis was carried out using locally fabricated flat plate solar collector setup, considering solar radiation data collected from the National Centre of Energy and Environment (NCEE), Benin City, Edo State, Nigeria. Using the same data set, ANSYS fluent 2018 version was employed for thermal simulation analysis to determine the flow within a serpentine tube, temperature and heat distribution across the flat plate as well as water temperature at the tube exit point. The model was developed to predict thermal behaviour of the system which in the process had considered the principles and laws of thermodynamics, while also solving the equations of continuity, momentum and energy. Water was assumed to be incompressible and flowing continuously while the flow was steady in nature and characterized by laminar. A significant correlation between the experimental and Computational Fluid Dynamics (CFD) simulated results was observed, as maximum experimental and CFD absorber plate temperatures of 368.64 and 372.98 k, serpentine tube water temperatures of 329.14 and 330.45 k and water outlet temperatures at tube exit of 330 and 329 k were obtained. The minimal temperature differential indicated an improved heat transfer absorber plate solar collector system. During the analysis, the physical and thermal properties of the absorber plate, tube and water were independent of the temperature. Heat loss from the base of the absorber plate bottom and the serpentine tube occurred via convection and depended on wind speed. Hence, adoption of ANSYS fluent is an effective CFD tool that can appropriately simulate thermally related problems in serpentine tube absorber plate solar collector system. The results obtained from both approaches were compared and analysed to validate the CFD model and gain insights into the system's performance.

1. INTRODUCTION

In other words, energy is an essential requirement for the growth and development of any given society. Therefore, its benefits to the wellbeing of man and its environs cannot be overemphasized (Ebunilo et al., 2018; Ikpe et al., 2019). Solar energy is one of the most available and reliable sources of

*Corresponding author, e-mail:author@fupre.edu.ng
DIO

renewable energy. It is also one of the renewable energy sources that has played an important role in the growth and development of many countries in the 21st century (Oselen et al., 2019; Riaz et al., 2022). Unlike hydroelectric and thermal energy, solar energy is abundant in Nigeria because of its geographical location near the equator (6 degrees from the equator). Southern Nigeria has about 5-7 hours of sunlight every day, and Northern Nigeria has about 9-11 hours of sunlight every day, which can be used as a sustainable energy source (Augustine and Nnabuchi, 2009; Owunna et al., 2018). The amount of solar radiation the Earth receives each year changes as the distance between the Earth and the Sun changes. The least distance between the Sun and the Earth is about 1. 71 x 10 m which occurs on December 21st, and is referred to as perihelion, while the highest distance is 1.512 x 1011 m which occurs on June 21st, and is known as aphelion (Robert et al., 2010). However, average distance between the Sun and Earth is known as the astronomical unit (AU), which is 1. 19 x 1011 m. The Earth rotating on its axis has an inclination of 23. 5 degrees with respect to its orbital plane axis (Yogi et al., 1999). This angle causes changes in solar radiation throughout the year. Therefore, due to new global environmental concepts and growing concerns about energy security and scarcity, developed countries have increased investment in renewable energy to replace conventional energy. The development of renewable energy can help solve challenges such as energy security, environmental pollution and climate change. In addition, renewable energy technologies are increasingly important for economic growth and job creation (Eronmosele et al., 2020). Today, the world is facing a new dimension in energy dynamics with the escalating effects of the war in Ukraine and the still ravaging Covid-19 pandemic, from which most economies are still they must be recovered. Discount (Markovska et al., 2016; Zhou et al., 2018; Farghali et al., 2023; Buonomano et al., 2023).

The use of new energy sources such as solar, wind and geothermal continues to grow and become more extensive. Flexible solar collectors, called PV/T collectors, use photovoltaic panels instead of specific heat sinks. Although the thermal efficiency of PV/T collectors may decrease slightly, better overall energy efficiency can be achieved because the solar cells can simultaneously generate electricity through the photovoltaic effect. The electrical efficiency of photovoltaic modules and the temperature of the cells are related. The working fluid can remove additional heat and improve the photoelectric conversion efficiency of the module (Zhou et al., 2017; Liu et al., 2018; Hayashi et al., 2018).

In addition, solar collectors are of unique importance in the green energy production value chain, as they can be used for water heating, drying of food items and other technical applications. On the other hand, several strategies (experimental and numerical) have been published to improve the efficiency of solar collectors (Al-Dabbas et al., 2021; Kumar et al., 2021). It should be noted that the report by Vengadesan and Senthil (2020) indicated that it is necessary to improve the shape and design parameters of the solar collector, improve the heat transfer between the heat transfer fluid (HTF) and the absorber tube and integrating the solar collector with phase change materials (PCM) under the absorbent plate. Their

experimental studies showed that the efficiency of solar collectors is significantly affected by the shape and composition of the absorber panels. This statement about the performance of heat absorption panels is also influenced by the thermal conductivity of the material, which is confirmed by the study of Douvi et al. (2021). Singh et al. (2010) estimated the total heat loss coefficient for different types of trapezoidal cavity absorbers with concentrator collectors with tubes and glass covers. The thermal performance of eight sets of linear concentrator trapezoidal absorbers at constant flow rate and temperature was evaluated and studied. Their analysis showed that the heat loss coefficient increased with absorption temperature and that the double glass cover also reduced the overall heat loss coefficient by 10-15% compared to a single glass cover. Fan et al. (2007) theoretically and experimentally proposed the flow and temperature changes in solar collectors with absorber plates made of horizontally inclined fins. A numerical study of flow velocity and heat transfer in solar panels using CFD calculations was also investigated. Experimentally, the flow distribution across the absorber was evaluated by temperature measurements at the bottom of the absorber. Their results showed good agreement between CFD results and experimental data at high flow rates. However, for lower flows, a significant difference was observed between the estimated and measured temperatures. This disagreement may be due to the simplification of the solar collector model.

Input data amassed from a prototype designed flat plate solar collector in Benin City was employed by Omo-Oghogho et al. (2021), in developing a model using energy balance method, which was computed with Explicit Finite Difference Method (EFDM) in MATLAB environment to predict thermal behaviour of the system. Outlet water temperature of 330 k, absorber plate temperature of 370 k and glass temperature 320 k were observed from the developed model. However, 0.05m, 0.06m and 0.07m were observed as the ideal insulation thickness while optimum design conditions for housing thickness were 0.020m, 0.024m and 0.026m.

In a similar study performed by Al-Manea et al. (2022), in Al-Samawa city, Iraq (Latitude 31.19 N and Longitude 5.17 E), the authors employed a Flat Plate Solar Collector (FPSC) with an inner absorber tube receiver in the investigation. At the site of the experiment, the ambient temperature and incident solar radiation were both 39 ^{o}C and 840 W/m^{2}.

They further employed a smooth copper tube with internal and exterior diameters of 9.5 and 12 mm, respectively, and a total length of 1000 mm was utilized in the prototype solar collector. Using the experimental data, a TRNSYS (Transient Simulation Software) model of a flat plate collector (prototype) combined with an absorber tube was created, simulated, and validated. Throughout the experiments, temperature and flow rate data were collected simultaneously to assess the effectiveness of the constructed solar collector. Both the water flow rate and the temperature at the solar collector input remained steady at 0.75 L/min and 37.7 C, respectively. The findings showed that the output temperature of the solar collector varied between 52 and 61 °C, with an average of 58 °C. The projected solar collector's efficiency ranges from about 45% and 67% respectively.

The declination angles, zenith angles, solar azimuth angles and the incident angles of Benin City, Edo State were obtained by Omo-Oghogho and Ikpe (2020), considering the ambient conditions, longitude and latitudes of site under consideration. This was achieved through experimental investigation using a prototype designed flat plate solar collector system. Average declination angle of 14.6675, average zenith Angles of the sun of 22.1850, average incidence angle of 21.7650, average solar Azimuth angle of 77.0625 and average ratio of beam radiation of 1.0875, with an average radiation of 1025.3258w/m^2 on a tilted surface were obtained. Similarly, Solar radiation data obtained through the use of an empirical model was employed by Omo-Oghogho et al. (2021), to predict and estimate solar radiation in Benin City, Edo State, Nigeria. The highest value of solar radiation was obtained in April, 2018 and the average horizontal radiation on a surface and radiation on tilted surface were 966.12 and 1055.99W/m^2 respectively. Thus this present study, is primarily focused on thermal analysis of a serpentine tube absorber plate solar collector system using experimental and CFD approach. This is premised on getting extremely effective solar collectors for homes and rural region utilities. Similarly, the system's net weight will be another consideration in the study apart from utilizing the prototype in power generation value chain.

2. MATERIALS AND METHOD

The experiment was aimed at determining the time and solar radiation required to obtain high temperature with significant efficiency from the designed and fabricated flat plate solar collector system for usage. The experimental set up also helped to validate the models CFD model developed. The experimental setup consisted of a serpentine tube absorber plate solar collector system, where a working fluid flowed through series of parallel tubes attached to an absorber plate. Temperature distribution along the absorber plate was measured using multiple thermocouples, while the outlet temperature of the working fluid was recorded. The solar collector was exposed to varying solar radiation levels, and the corresponding temperature data was collected for analysis. To complement the experimental findings, a CFD model was developed to simulate the fluid flow and heat transfer within the serpentine tube absorber plate solar collector system. The CFD model incorporated governing equations of fluid dynamics and heat transfer, along with appropriate boundary conditions. The model is validated by comparing the simulation results with the experimental data obtained earlier. All the components of the FPSC were gathered and assembled together. The arrangement was positioned in an open place under a clear sky atmosphere at the mid-months. Cleaning of the absorber plate, flow tube and glazing cover was done to remove dust particles and moisture content. The cold water supply tank was filled with fresh and clean water and placed at a height of one and half meter (0.5m) from the FPSC inlet as shown in the experimental setup in Figure 1.

Figure 1: Experimental setup of the flat plate solar collector

The collector was exposed to the sun from 8 am to 12 pm, this process of exposing the flat plate solar collector to the sun before passing water through it was termed preheating the collector system. Preheating the solar collector was done from 8am to 12noon for January, February, March etc. as dry season and June, July, September etc, as rainy season respectively. While the water passed through the collector, the inlet temperature and the outlet temperature of water was recorded using thermocouples. The solar radiation was also recorded using a solar meter. Mass Flow Rate (MFR) of water was measured by observing the time required for the collection of 600ml water using measuring jar and stop watch (45 seconds). Each experiment was conducted for 1 hour duration by maintaining constant flow rate of water. The readings were taken after every hour and a mass flow rate of 0.0133kg/s gotten after 45sec.

To carry out the experimentation using the designed flat plate solar collector, the amount of solar radiation, day, declination angle, zenith angle of the sun, azimuth angle and the angle of incidence on the inclined surface was determined. A particular day in each month was selected (mid-month), which had approximately the total solar radiation which is equal to the monthly mean value for that particular month (Klein, 1977). To design the FPSC, the area was determined considering the temperature of fluid (water) expected and the expected solar radiation of the location. The heat requirement is a function of the mass flow rate and the time of heating. Figure 2 shows an isometric view of the flat plate solar collector experimental set-up tilted at 10^{o} and has a water supply tank and a water discharge tank. The materials used in the flat plate solar collector setup were wood used for casing, fibre (Polyurethane) used for insulation, aluminium painted black used for absorber plate, copper used for flow tube, transparent glass used for glazing cover, plastic used for water supply and discharged tank, plastic hose used for connecting the water tanks. The various components, materials and dimensions for prototype of the experimental setup are presented in Table 1.

*Corresponding author, e-mail:author@fupre.edu.ng
DIO

Table 1: Materials and dimensions of flat plate solar collector design setup

S/N	Components	Materials	Dimensions
1	Casing	Wood	0.84m × 0.79m × 0.08m
2	Insulation	Fiber (Polyurethane)	0.80m × 0.75m × 0.004m
3	Absorber plate	Aluminum painted black	0.80m × 0.75m
4	Flow tube	Copper	0.012m in diameter
5	Glazing cover	Transparent glass	0.80m × 0.75m × 0.005m
6	Water supply tank	Plastic	300 liters
7	Hot water collecting tank	Plastic	20 liters
8	Pipe	Plastic hose	h =1m , d=0.008mm

The following initial conditions were considered for the flat plate solar collector system.

i. Steady state system.
ii. 26.1^{o}C daily average water inlet temperature which was ambient temperature obtained from the National Centre for Energy and Environment (NCEE), Benin City, Edo State, Nigeria.
iii. Active heating time of the water is estimated to be about 6 hours, within which the sun is actively present. Though daily peak temperature may vary with time.
iv. 100^{o}C absorber plate temperature.
v. Average daily solar radiation I = 1017.695W/m^2 from NCEE, University of Benin.
vi. Specific heating capacity of water Cp = 4190J/kgK.
vii. Tilt angle of 10^{o}
viii. 300 litres capacity water tank was used to supply water to the solar collector. The tank was placed at 0.5m height from the collector inlet, thus creating the required pressure head for circulation of water in the system.
ix. The surface azimuth angle is 0^{o} (the collector is facing the south).
x. The solar parameters are calculated with the sun one hour after noon i.e. 15^{o}.

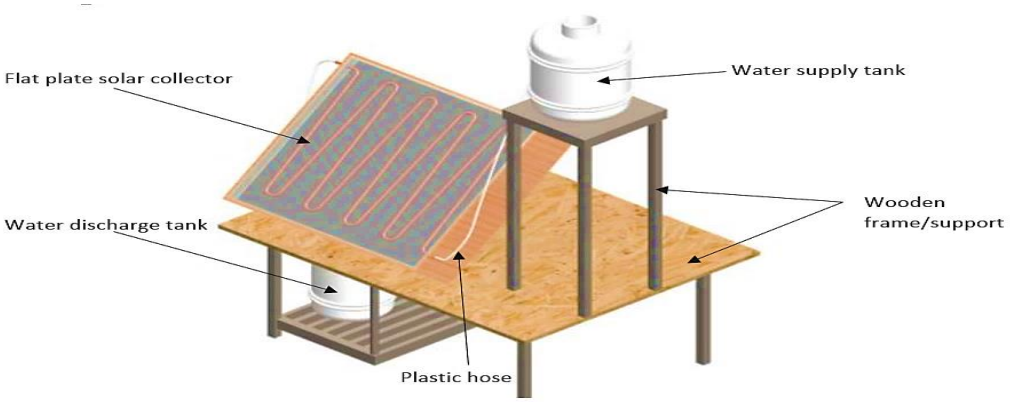

Figure 2: Flat plate solar collector setup

2.1. Thermodynamic Equations

Thermodynamic equations employed in computing the solar collector parameters are as follows:

A. Declination angle

To effectively estimate the solar radiation of a tilted surface, there is need to know the angular position of the sun at solar noon, hence the determination of the declination angle considering the number of days. Declination angle varies and is calculated using the following relation in Equation 1.

$$\delta = 23.45\, sin\left(360\,\frac{284+n}{365}\right) \quad (1)$$

where n is the no of days. For n, the mean day in each month was used.

B. Zenith Angles of the sun

The Zenith angle was estimated considering the angle between the vertical and the line to the sun, that is, the angle of incidence of beam radiation on a horizontal surface has to be known in order to effectively estimate the amount of solar radiation on a solar collector. The zenith angle is given by Equation 2:

$$cos\,\theta_z = cos\,\phi\, cos\,\delta\, cos\,\omega + sin\,\phi\, sin\,\delta \quad (2)$$

where Φ = 6.5438^o (Latitude of Benin City, Edo State, Nigeria), δ = declination angle, ω = Hour angle (15^0 was used because 1pm was considered as the time, during the system analysis)

C. Solar Azimuth Angle (γ_s)

The solar azimuth angle is estimated using the following relations in Equation 3:

$$\gamma_s = sin(\omega)\left|cos^{-1}\left(\frac{cos\,\theta_z\, sin\,\phi - sin\,\delta}{sin\,\theta_z\, cos\,\phi}\right)\right| \quad (3)$$

where, Sign function is used to determine ω, θ_z = Zenith angle, ϕ = lattitude of site and δ = Declination angle.

D. Incidence angle

The angle of incidence on the inclined surface is given by Equation 4 (Duffie and Beckman, 2013):

$$cos\,\theta = cos\,\theta z\, cos\,\beta + sin\,\theta z\, sin\,\beta\, cos\,(\gamma s - \gamma) \quad (4)$$

Where θ = incidence angle, β = tilted angle, $\gamma = 0, because\ it\ is\ facing\ south$, θz = Zenith angle and γs = Solar azimuth angle.

E. Radiation on tilted surface

The data collected from the National Centre for Energy and Environment (NCEE) Benin, Edo State, Nigeria (NCEE, 2017), are related to the horizontal surface, for purposes of solar process design and performance calculations, it is often necessary to calculate the radiation on a tilted surface of a collector from measurements or estimates of solar radiation on a horizontal surface. The geometric factor R_b, is the ratio of beam radiation on the tilted surface to that on a horizontal surface and this can be estimated using the following relations in Equation 5.

*Corresponding author, e-mail:author@fupre.edu.ng
DIO

$$R_b = \frac{Cos\,\theta}{Cos\theta_z} = \frac{G_{b,t}}{G_h} \quad (5)$$

where θ = angle of incidence, θ_z = zenith angle respectively, $G_{b,t}$ = radiation on tilted surface and G_h = radiation on horizontal surface.

To utilize R_b the radiation on the horizontal surface was gotten from NCEE (2017). To determine the available energy in the solar collector, it is important to consider the equation for energy gained by the working fluid. This is given by Equation 6 (Al-Sulaiman, 2014):

$$Q_{use} = m_a C_p \Delta T \quad (6)$$

Equation for heat losses from the collector as the fluid flows from the solar collector to the atmosphere is expressed in Equation 7 (Islam et al., 2015):

$$Q_{use} = A_{abs} Q_r [S_i - U_1\,(\Delta T)] \quad (7)$$

The energy leaked from the solar collector is given by Equation 8 (Calise et al., 2016):

$$E_1 = \left\{U_1 A_{abs}(T_{abs} - T_a)\,\left(1 - \frac{T_a}{T_{abs}}\right)\right\} \quad (8)$$

where S_i is the optical absorbed solar flux and U_l is the heat loss by emittance, reflection and optical efficiency of glazing given by Equation 9 (Jafarkazemi and Ahmadifard, 2013):

$$Q_R = \frac{maC_P}{U_1 A_{abs}}\left[1 - exp\left\{\frac{-F\emptyset U_1 A_{abs}}{maC_P}\right\}\right] \quad (9)$$

The energy destroyed by the solar collector is given by Equation 10 (Farahat et al., 2009):

$$E_d = -mC_P T_a \frac{T_{out}}{T_{in}} E_d = -mC_P T_a \left\{1n\left(\frac{T_{out}}{T_{in}}\right) - \left(\frac{T_{out} - T_{in}}{T_{abs}}\right)\right\} \quad (10)$$

where E_d is the heat loss due to absorber plate temperature difference with the fluids. It is the latent heat absorbed by the fluids in phase change. The exergy of the solar collector is given by Equation 11 (Islam et al., 2015):

$$E_{out} = \left[\left\{\left(m_a C_P\left(T_{out} - T_a T_a l_n \frac{T_{out}}{T_a}\right) - \frac{m\Delta P_{out}}{\rho}\right) + mwC_P(T_w - T_a)\right\}\right] \quad (11)$$

The discharge flow rate of water expressed in m^3/sec is given by Equation 12:

$$Q = \frac{\pi}{4} d^2 v \quad (12)$$

where d is the diameter of the collector pipe and v is the average velocity of fluid. In this case, the angle of incidence is given by Equation 13 (Kalogirou et al., 2016):

$$Cos\theta = Sin\emptyset\,(Sin\delta\,Cos\beta + Cos\delta\,Cos\gamma\,Cos\omega\,Sin\beta) + Cos\emptyset\,(Cos\delta\,Cos\omega\,Cos\beta - Sin\delta\,Cos\gamma\,Sin\beta) + Cos\delta\,Sin\gamma\,Sin\omega\,Sin\beta \quad (13)$$

where δ is the Declination angle, n is no of day in the yea, β is the slope angle $\emptyset$ is the latitude of the location γ is the surface azimuth angle and ω is the hour angle. Tilt factor for beam radiation is given by Equation 14.

$$rr_b = \frac{Cos\theta}{Cos\theta_z} \quad (14)$$

$$Cos\theta_z = (Sin\emptyset * Sin\delta) + (Cos\emptyset * Cos\delta * Cos\omega) \quad (15)$$

Radiation shape factor for the diffused radiation is given by Equation 16 while the tilt factor for reflected radiation is given by Equation 17.

$$R_d = \frac{(1+Cos\beta)}{2} \quad (16)$$

$$r_r = \frac{\rho(1-Cos\beta)}{2} \quad (17)$$

Instantaneous efficiency is given by Equation 18 while exergy (e) is given by Equation 19

$$\eta_i = \frac{\dot{m}C_P(T_2-T_1)}{I_t * A_p} \quad (18)$$

$$e = (h-h_o) - T_o(S-S_o) + \frac{V^2}{2} + gz \quad kJ/kg \quad (19)$$

The top loss coefficient is given by Equation 20.

$$U_T = \left(\frac{N}{\frac{C}{T_{pm}}\left[\frac{(T_{pm}-T_a)}{(N+f)}\right]^e} + \frac{1}{h_w}\right)^{-1} + \frac{\sigma(T_{pm}+T_a)(T_{pm}^2+T_a^2)}{\frac{1}{\varepsilon_p+0.00591Nh_w} + \frac{2N+f-1+0.133\varepsilon_p}{\varepsilon_g} - N} \quad (20)$$

Where f = focal distance, h_w= wind heat transfer, ε_p= emittance of plate, N = number of glass covers, c = collector factor, e = emissive power, ε_g= emittance of glass (0.88), T_a = ambient temperature and T_{pm}= mean plate temperature. The bottom loss coefficient is given by the relation in Equation 21:

$$U_B = \frac{k}{L} \quad (21)$$

Where k is thermal Conductivity (Urethane) = 0.028 and L = thickness of urethane layer = 30mm = 0.03. Edge loss coefficient can was estimated using Equation 22:

$$U_e = \frac{\frac{k}{L_e} \times P \times C_t}{C_A} \quad (22)$$

Where k = thermal conductivity of insulation (polyurethane), L_e =Thickness of edge insulation, P = Perimeter of collector, C_t = Thickness of Collector, C_A = Collector Area. The useful energy is given by Equation 23.

$$Q_u = A_c(S - U_L(T_{pm} - T_A) \quad (23)$$

The bond conductance C_b is given by Equation 24.

$$C_b = \frac{K_b b}{\gamma} \quad (24)$$

Where K_b is the bond conductivity, b = bond Width and γ = Bond Thickness. The radiation tilted surface derived from the angle of incidence on the inclined surface is given by Equation 25.

$$R_b = \frac{\text{Cos}\,\theta}{\text{Cos}\theta_z} \quad (25)$$

The amount of solar energy received by the collector can also be obtained by the product of the rate of transmission of the

glass cover and the absorption rate of the absorber and this is substituted in Equation 26.

where Q_{rec} is the solar energy received, τ is the transmissivity and ε is the absorption rate. As the collector absorbs heat its temperature gets higher than that of the surrounding and heat is lost to the atmosphere by convection and radiation. The rate of heat loss depends on the collector overall heat transfer coefficient, collector temperature and ambient temperature respectively. This is represented mathematically by Equation 27.

$$Q_{loss} = U_T A(T_p - T_a) \quad (27)$$

where Q_{loss} is the heat loss, U_T is the overall heat transfer coefficient, T_p is initial temperature of the absorber plate and T_a is the ambient temperature respectively. Thus the rate of useful energy extracted by the collector is the rate of extraction under steady state conditions and it is proportional to the useful energy absorbed by the collector. This is given by Equation 28a-b.

$$Q_{usfl} = Q_{recv} - Q_{loss} = I_n\, A(\tau\varepsilon) - hA(T_p - T_a) \quad (28a)$$

$$Q_{usfl} = mC_P(T_p - T_a) \quad (28b)$$

where Q_{usfl} is heat energy gained by the fluid, *m* is the mass flow rate of the fluid and C_p is the specific heat capacity of the fluid and the heat removal factor F_R is given by Equation 29.

$$F_R = \frac{\dot{m}C_p(T_{out} - T_{in})}{A((\tau\varepsilon) - h(T_p - T_a)} \quad (29)$$

$$Q_{usfl} = AF_R\left[I_n(\tau\alpha)_{av} - U_L(T_p - T_a)\right] \quad (30)$$

$$\frac{Q_{usfl}}{A} = q = I_n(\tau\varepsilon) - h(T_p - T_a) \quad (31)$$

2.2. CFD Simulation

The CFD simulation was carried out using ANSYS Fluent 2018 version. It was used to determine the water outflow temperatures and the heat distribution on the absorber plate, the equation for continuity, momentum and energy were considered. The geometry was designed using ANSYS and the model was subjected to meshing for accuracy, convergence and speed of simulation. Parameters of the geometry were also defined. To enhance thermal and flow analysis, fining was selected under the meshing size to discretize the flow into many elements and it is then updated to recognize the input. The properties of the materials employed for the model were activated from the domain, the properties of water was used for the liquid domain in the computational mesh. Piece-linear functions were considered to take into account the dependence of water properties on temperature, effects of gravity was also taken into account along the vertical axis and since the flow was very small, laminar flow model with pressure-velocity coupling was used.

On the computational domain, the width, length, thickness, thermal conductivity of the absorber plate, thermal conductivity of the pipe material, solar radiation and temperatures were considered. The domain

discretization was done considering a structured grid consisting of hexahedral elements of 0.6mm for the fluid part and 1mm for the solid part, the number of registered elements in the mesh for the computational domain consisting of water, water pipe and absorber plate were 522800 as presented in the mesh diagram of the collector system in Figure 3. Input parameters used for the modelling are presented in Table 2

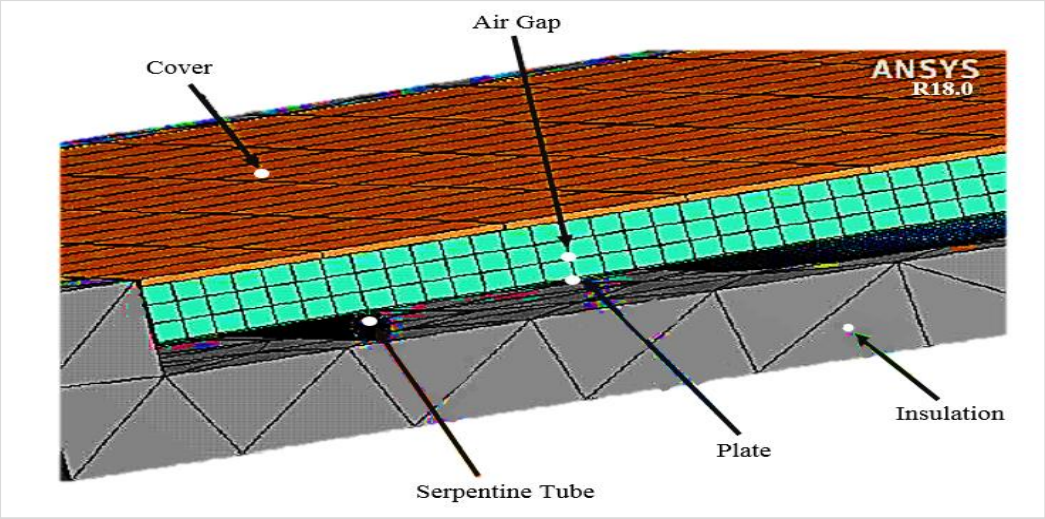

Figure 3: Mesh diagram of the collector system

Table 2: Initial input parameters for the model

Parameters	Value
Emmitance of plate	0.84
Emissivity of glass	0.04
Heat capacity of glass (KJ/kg.K)	0.80
Heat capacity of absorber plate (kJ/kg.K)	0.90
Heat capacity of water (KJ/kg.k)	4.18
Area of collector (m^2)	0.84
Area of fluid pipe (m^2)	0.047
Insulation thickness (m)	0.05
Housing thickness (m)	0.02
Mass of glass (kg)	18.8
Mass of absorber plate (kg)	8.93
Mass flow rate (kg/s^2)	0.03
Wind velocity (m/s)	1.648
Initial glass temperature (k)	315
Initial water inlet temperature (k)	305
Initial housing temperature (k)	315
Initial insulation temperature (k)	325
Thermal conductivity of insulation (glass wool) (W/mk)	0.034
Thermal conductivity of housing (W/mk)	0.12
Thermal conductivity of air (W/mk)	0.024
Thermal conductivity of copper (W/mk)	386
Thermal conductivity of aluminium (W/mk)	239
Transmittance of glass	0.94
Radiation on a tilted surface (W/m^2)	937.18

3. RESULTS AND DISCUSSION

Using the thermodynamic equations in shown earlier, the following parameters in Table 3 were computed as follows:

Table 3: Parameters computed from thermodynamic equations

Declination angle (δ)	-20.961
Zenith angle (θ_z)	31.16°
Solar azimuth angle (γ_s)	-27.82
Angle of incidence on inclined surface (θ)	22.75
Radiation tilted surface (R_b)	1.08
Wind heat transfer (h_w)	9.505 W/m^2C
Mean plate temperature (T_{pm})	373 K
Ambient temperature (T_a)	299.1k
Emissive power (e)	0.315
Collector factor (c)	517
Focal distance (f)	0.855
Top loss coefficient (U_T)	6.33 W/m^2℃
Bottom loss coefficient (U_B)	0.933 W/m^2℃
Edge loss coefficient (U_e)	0.56 W/m^2℃
Useful energy (Q_u)	328.36 W
Overall loss coefficient	7.82 W/m2 ^oC.
Plate thermal conductivity (Aluminium)	235 W/m^{2o}C
Heat transfer coefficient inside Tubes	300 W/m^2 ^{o}C
Bond conductivity (C_b)	386 W/m^2 ^{o}C
Collector mass flow rate	0.014 kg/s
Collector flow factor (F_f)	0.271
Outlet fluid temperature	334 k
Instantaneous efficiency (η_i)	0.474

Figure 4 shows the plot of experimental absorber plate temperature with time, which indicates that the temperature distribution on the absorber plate within a time frame of 200 seconds. From the plot, maximum absorber plate temperature of about 370 k was obtained at maximum time of 200 s. Figure 5 shows the experimental temperature of serpentine tube with time. From the plot, thermal behaviour of the serpentine tube, revealed maximum serpentine tube temperature of 330 k at a maximum experimental time of 200 seconds. Figure 6 shows the experimental water outlet temperature at the serpentine tube exit with time. Like the case in Figure 5, this indicated that a maximum serpentine tube exit temperature of 330 k was obtained at a maximum experimental time of 200 seconds. Comparing the temperature of the serpentine tube with time and the temperature of water outlet at the serpentine tube exit with time, it can be observed that they are practically the same with zero difference. This implies that there was no heat loss in the system, as the temperature of water along the serpentine tube still maintained the same temperature at the tube exit. This is also an indication of the efficiency of the system.

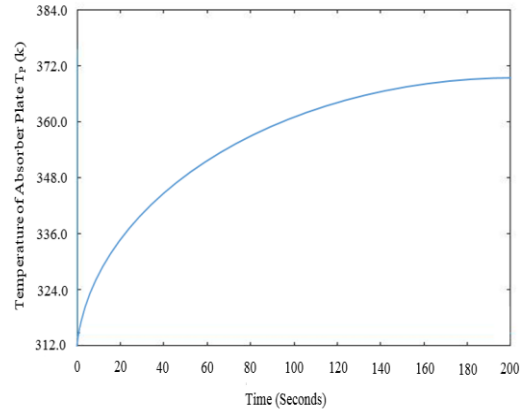

Figure 4: Experimental temperature of absorber plate with time

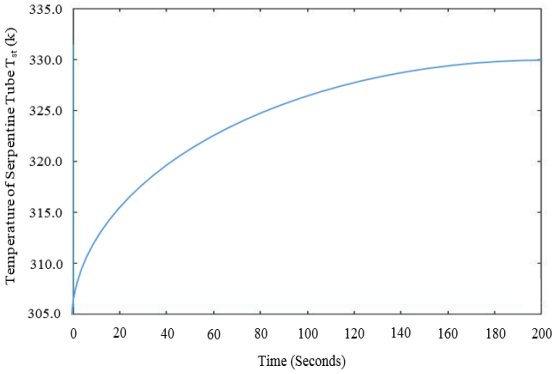

Figure 5: Experimental serpentine tube water temperature with time

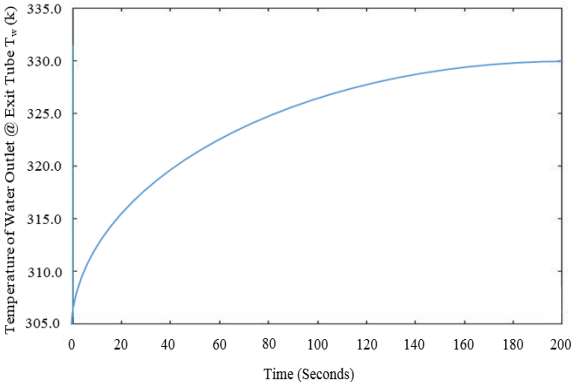

Figure 6: Experimental water outlet temperature at tube exit with time

Parameters (see Table 2) considered during the model development of the system were used for determining the temperature distribution along the absorber plate and the flow pipe. The main point of focus were on the absorber plate and water flow pipes. The temperature distribution on the absorber plate and the water flow pipes obtained from the simulated model is shown in Figure 7a. The maximum temperature obtained is 371.77 k while the minimum temperature is 310.45. The temperature is observed to be higher on the absorber plate than temperature on the water flow pipes. Temperature of the absorber plate with serpentine tubing was further simulated for about 350 iterations as shown in Figure 7b. The graphical representation is characterised by sinusoidal patterns, due to the increasing and decreasing heat intensity along the absorber plate as a result of inconsistencies in sunlight. Figure 8 shows the temperature profile of water distribution along the serpentine tubing. Maximum and minimum temperature of about 381 and 310.45 k was achieved. Using the input data in Table 2, the simulation was carried with solar radiation of 937.18W/m^2 on tilted surface.

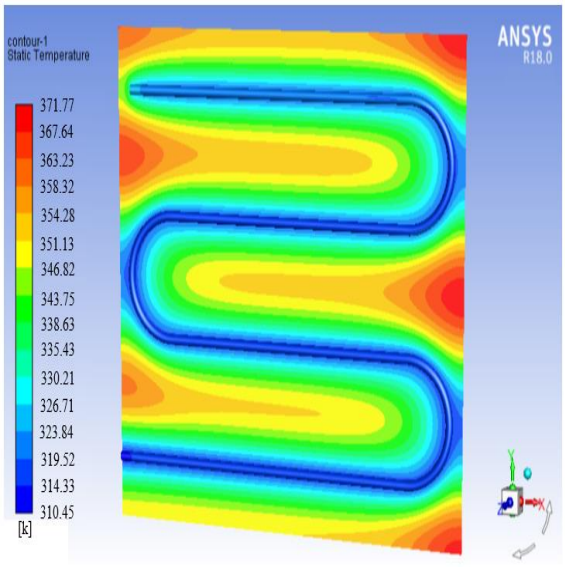

Figure 7a: Temperature contour of the absorber plate with the serpentine tubing

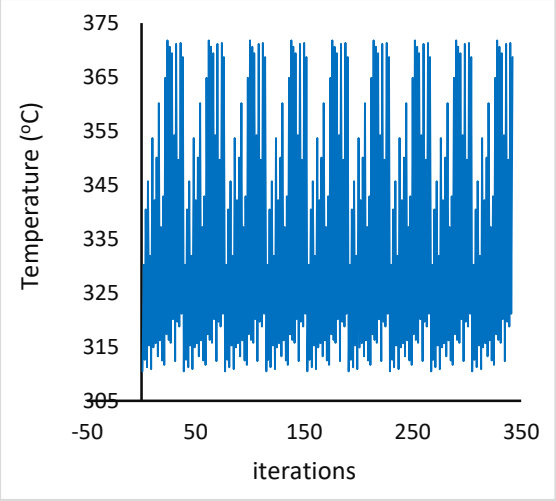

Figure 7b: Temperature of the absorber plate with serpentine tubing at various iterations

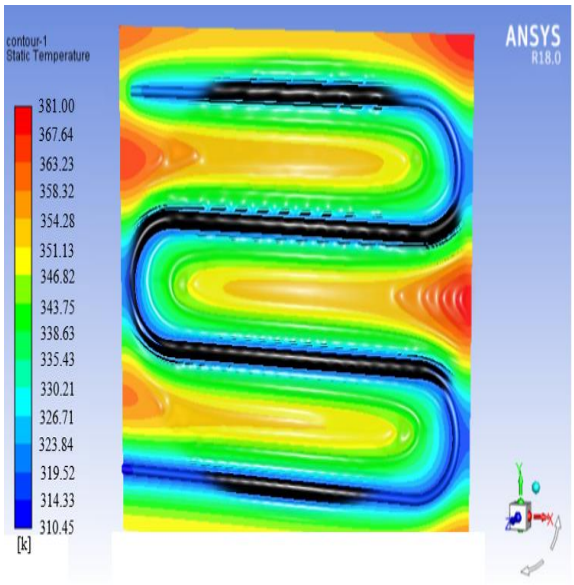

Figure 8: Temperature profile of water along the serpentine tubing

Figure 9a represents temperature simulation profile of the serpentine tubing. Water entered the tube at an inlet temperature of 305.13 k and as it moves through the tube to the exit, the temperature increases to 330.45 k. This result shows that the heat transfer between the absorber plate and the flow pipe is good and also demonstrate that the parameters for the design of the solar collector can bring about improvement in the system performance. The profile in Figure 9a is graphically presented in Figure 9b, being simulation temperature of water along the serpentine tubing at various iterations. Also, the plot is characterised by sinusoidal patterns, due to the increasing and decreasing heat intensity along the absorber plate as a result of inconsistencies in sunlight.

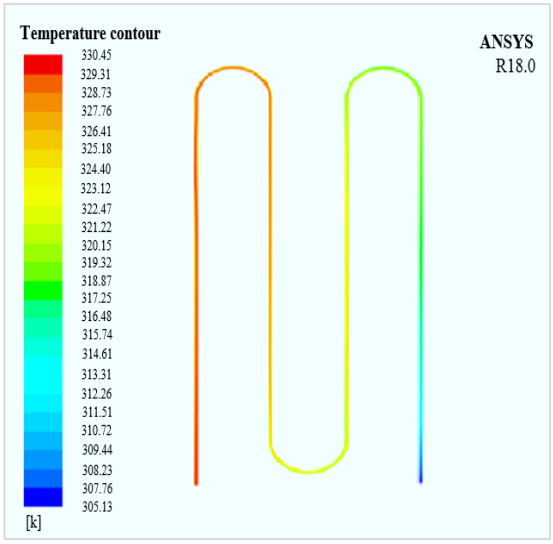

Figure 9a: Temperature contour of the serpentine tubing

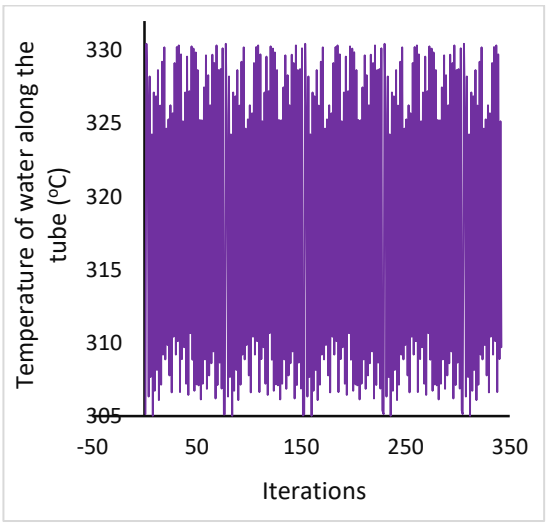

Figure 9b: Temperature of water along the serpentine tubing at various iterations

Figure 10a shows the temperature distribution across the surface of the absorber plate. At the beginning of the

simulation a temperature of 309.11 k was obtained. At the end of the simulation, a temperature of 372.98 k was achieved. This is relatively high and as such indicates an improvement in the collector performance. The profile in Figure 10a is graphically presented in Figure 10b, being simulation temperature of the absorber plate at various iterations. The plot is characterised by sinusoidal patterns, due to the increasing and decreasing heat intensity along the absorber plate as a result of inconsistencies in sunlight.

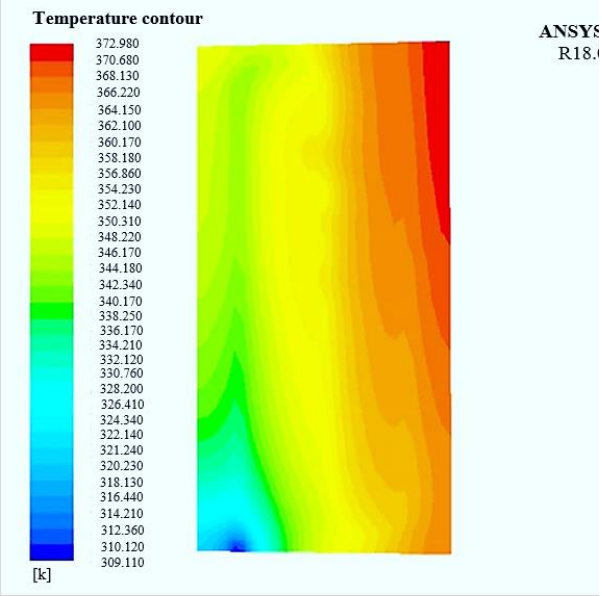

Figure 10a: Temperature contour of the absorber plate

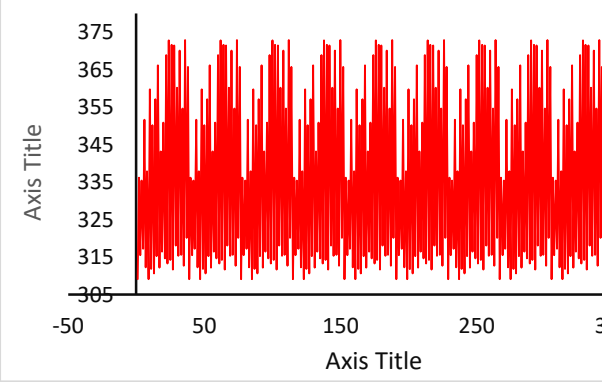

Figure 10b: Temperature of the absorber plate at various iterations

Figure 11a shows the temperature profile of water at the serpentine tube exit. Using the input data in Table 2, the simulation was carried out which shows that water entered the flow pipe at a temperature of 305.13 k, and increased to a temperature of 329.96 k at the exit. The differential temperature indicated an improved heat transfer system that minimized losses as the fluid travelled along the tube while allowing increase in the fluid temperature. Temperature of water outlet along the serpentine tube exit was simulated at various iterations and graphically presented in Figure 11b. The plot is characterised by sinusoidal patterns, due to the increasing and decreasing heat intensity along the serpentine tube as a result of inconsistencies in sunlight.

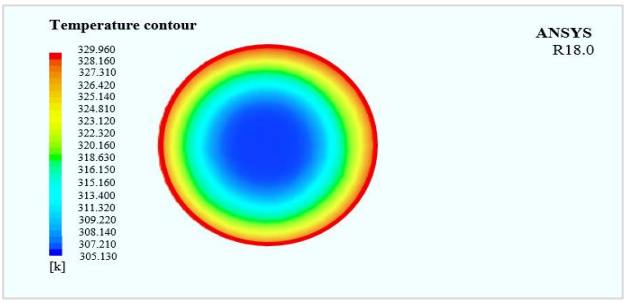

Figure 11a: Temperature of water outlet in serpentine tube exit

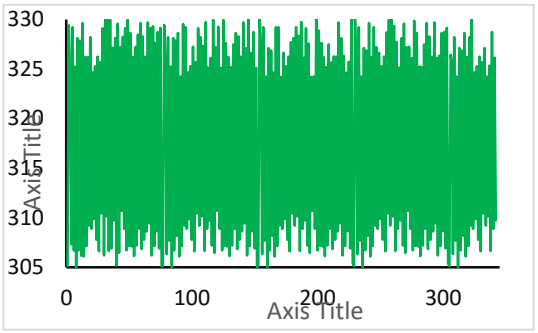

Figure 11b: Temperature of water outlet in serpentine tube exit at various iterations

Figure 12a represents a plot of maximum experimental and CFD serpentine tube water temperatures. From the plot, maximum and minimum serpentine tube

temperature obtained experimentally and via CFD simulation were recorded as 329.14 and 330.45 k as well as 305 and 305.13 k. A significant correlation is observed between the values obtained both from the experimental approach and the CFD simulation. The temperature difference in this case is negligible, which is an indication of that CFD is an appropriate tool that can be employed in thermally related simulation of this nature.

Figure 12b represents a plot of experimental and CFD absorber plate temperatures. From the plot, maximum and minimum serpentine tube temperature determined experimentally and through CFD approach were as 368.64 and 372.98 as well as 312 and 309.11 k respectively. Comparing the minimum and maximum temperature values of the serpentine tube, the difference is not much but higher than those obtained in the previous plot in Figure 12a. Although the differences are more than 1 k, they are not more than 5 k, which still fells within a workable range.

Figure 12c represents a plot of experimental and CFD water outlet temperatures at serpentine tube exit. From the plot, maximum and minimum serpentine tube temperature obtained experimentally and via CFD simulation were recorded as 330 and 329.96 k as well as 305 and 305.13 k. Like the case of Figure 12a, the correlation between experimental and CFD simulation results is about 99%, indicating the effectiveness of CFD simulation in thermally related analysis of a serpentine tube absorber plate solar collector system.

Figure 12d represents a plot of multiple simulated temperature output using CFD approach. In other words, comparison of maximum CFD simulated output temperatures which included maximum water outlet temperature of 329.96 k, maximum temperature of absorber plate of 372.98 k, maximum temperature of serpentine tubing of 330.45 k, maximum temperature of water along serpentine tube of 381 k and maximum temperature of absorber plate with serpentine tube of 371.77 k respectively. Comparably, the experimental and CFD results obtained in this paper agrees with similar studies conducted by Kebede (2016), Saleh (2012), Kurri (2018), Muhammad et al. (2018) and Gond et al. (2016).

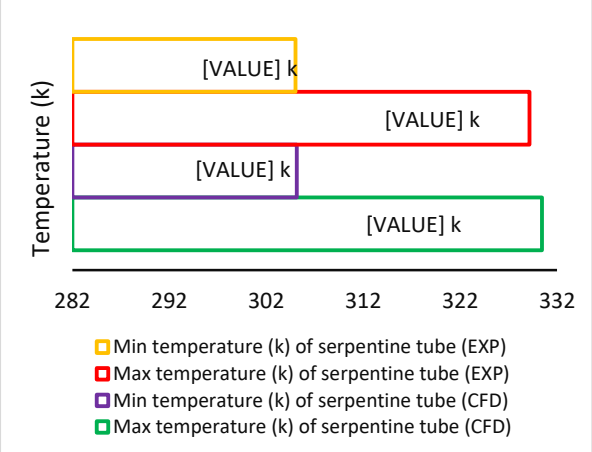

Figure 12a: Maximum experimental and CFD serpentine tube water temperatures

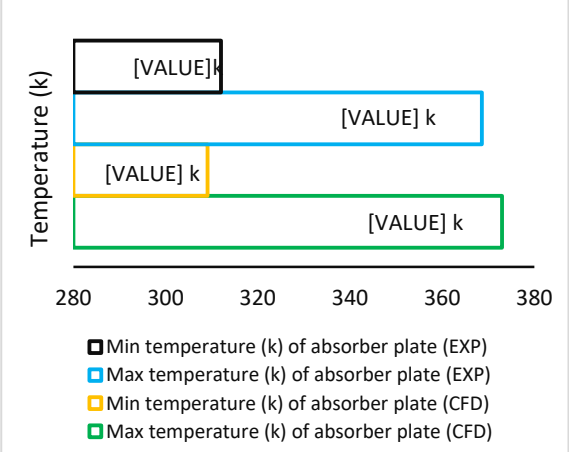

Figure 12b: Plot of experimental and CFD maximum absorber plate temperatures

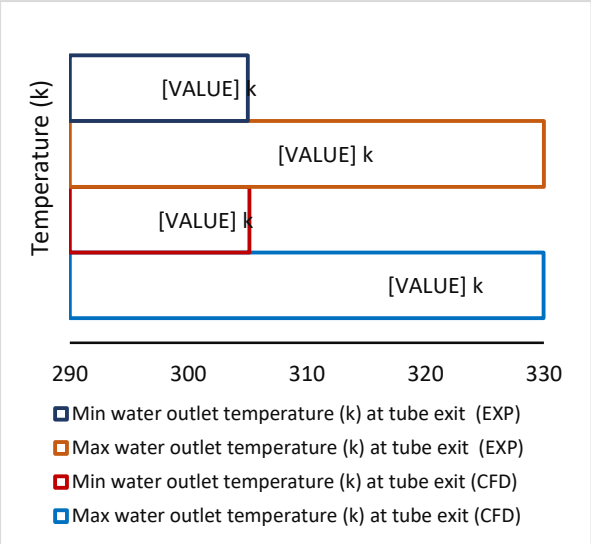

Figure 12c: experimental and CFD maximum water outlet temperatures at tube exit

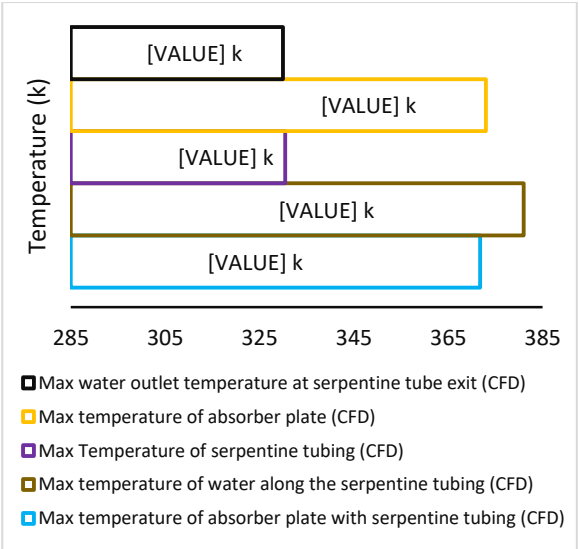

Figure 12d: Multiple simulated maximum temperatures output using CFD approach

Solar collectors are widely used to convert solar radiation into usable thermal energy. Among various collector designs, the serpentine tube absorber plate solar collector system offers several advantages, including a large surface area for heat absorption and efficient heat transfer. Understanding the thermal behaviour of such a system is crucial for optimizing its performance and enhancing its efficiency. The experimental results provided insights into the temperature distribution along the absorber plate and the outlet temperature of the working fluid under different solar radiation levels. The CFD simulations offered a detailed understanding of the fluid flow patterns, velocity profiles, and heat transfer mechanisms (Ikpe et al., 2018; Ikpe et al., 2021), within the collector system. Comparison between the experimental and CFD results demonstrated the accuracy and reliability of the CFD model in predicting the system's thermal behaviour. The experimental setup involved measuring the temperature distribution along the absorber plate and the outlet temperature of the working fluid. The CFD simulations carried out to obtain a detailed understanding of the fluid flow and heat transfer characteristics within the collector system.

4. CONCLUSION

The thermal analysis of a serpentine tube absorber plate solar collector system in south-south Nigerian environs using experimental and CFD approach was success fully carried out in this study. The system design, thermodynamic analysis, modelling, simulation and experimental determination of the output temperature, retained energy as well as efficiency of the solar flat plate collector, and the results obtained have shown a correlation of the methods. A computational model was also developed to predict more accurately the output temperature and efficiency of the output water leaving a flat plate solar collector. The model provided more realistic assumptions and simplified approach to studying the behaviour of a flat plate collector system. Considering the outcome of the study, it can be deduced

that the experimental and CFD predicted results are close with significant correlation, indicating that the model can simulated the performance of the system beyond experimental boundaries. The thermal analysis of a serpentine tube absorber plate solar collector system using experimental and CFD approaches has provided valuable insights into the system's performance. The experimental measurements and CFD simulations complement each other, enabling a comprehensive understanding of the fluid flow and heat transfer characteristics within the collector system. The validated CFD model can be further utilized for optimizing the system design and enhancing its efficiency. This study contributes to the advancement of solar collector technology and promotes the utilization of solar energy as a sustainable energy source.

Abbreviations

n Number of days
Φ Latitude of Benin City, Edo State, Nigeria
δ Declination angle
ω Hour angle
F_f Collector flow factor
γs Solar Azimuth Angle
θ_z Zenith angle
ϕ latitude of site
θ Incidence angle
β Tilted angle
R_b Geometric factor
$G_{b,t}$ Radiation on tilted surface
G_h Radiation on horizontal surface
S_i Optical absorbed solar flux
U_l Heat loss by emittance, reflection and optical efficiency of glazing.
E_d Heat loss due to absorber plate temperature difference with fluid
d Diameter of the collector pipe
v Average velocity of fluid
η_i Instantaneous efficiency
e Exergy, Emissive power
f Focal distance
h_w Wind heat transfer
ε_p Plate emittance
N Number of glass covers
c Collector factor
ε_g Glass emittance
T_a Ambient temperature
T_{pm} Mean plate temperature
k Thermal conductivity
L Thickness of urethane layer
L_e Thickness of edge insulation
P Perimeter of collector
C_t Thickness of collector
C_A Collector area
K_b Bond conductivity
b Bond width

γ	Bond thickness
Q_{rec}	Solar energy received
τ	Transmissivity
ε	Absorption rate
Q_{loss}	Heat loss
U_T	Overall heat transfer coefficient
T_p	Initial temperature of absorber plate
T_a	Ambient temperature
Q_{usfl}	Heat energy gained by the fluid
m	Mass flow rate of the fluid
C_p	Specific heat capacity of the fluid
F_R	Heat removal factor
Q_u	Useful energy
U_e	Edge loss coefficient
U_T	Top loss coefficient
R_b	Radiation tilted surface
NCEE	National Centre of Energy and Environment
CFD	Computational Fluid Dynamics
AU	Astronomical Unit
HTF	Heat Transfer Fluid
PCM	Phase Change Material
EFDM	Explicit Finite Difference Method
FPSC	Flat Plate Solar Collector
TRNSYS	Transient Simulation Software
MFR	Mass Flow Rate
NCEE	National Centre for Energy and Environment

Reference

Al-Dabbas, M., Alahmer, A., Mamkagh, A. and Gomaa, M.R., (2021). Productivity enhancement of the solar still by using water cooled finned condensing pipe. Desalination Water Treat, 213, 35-43.

Al-Manea, A., Al-Rbaihat, R., Kadhim, H.T., Alahmer, A., Yusaf, T. and Egab, K., (2022). Experimental and numerical study to develop TRANSYS model for an active flat plate solar collector with an internally serpentine tube receiver. International Journal of Thermofluids, 15, 100189.

Al-Sulaiman, F.A. (2014). Exergy analysis of parabolic trough solar collectors integrated with combined steam and organic Rankine cycles. Energy Conversion and Management, 77, 441-449.

Augustine C. and Nnabuchi M.N. (2009). Relationship between Global Solar Radiation and sunshine Hours for Calabar, Port Harcourt and Enugu, Nigeria. International Journal of Physical Sciences, 4 (4), 182-188.

Buonomano, A., Barone, G. and Forzano, C., (2023). Latest advancements and challenges of technologies and methods for accelerating the sustainable energy transition. Energy Reports, 9, 3343-3355.

Calise, F., d'Accadia, M.D., Macaluso, A., Piacentino, A. and Vanoli, L., (2016). Exergetic and exergoeconomic analysis of a novel hybrid solar-geothermal polygeneration system producing energy and water. Energy Conversion and Management, 115(1), 200-220.

Douvi, E., Pagkalos, C., Dogkas, G., Koukou, M.K., Stathopoulos, V.N., Caouris, Y., and Vrachopoulos, M.G., (2021). Phase change materials in solar domestic hot water systems: A review. International Journal of Thermofluids, 10, 100075.

Duffie, J.A. and Beckman, W.A., (2013). Solar Engineering of Thermal Processes. John Wiley and Sons Inc, New York.

Ebunilo, P.O., Okovido, J. and Ikpe, A.E., (2018). Investigation of the energy (biogas) production from co-digestion of organic waste materials. International Journal of Energy Applications and Technologies, 5(2), 68-75.

Eronmosele, P., Akhihiero, E.T. and Ikpe, A.E., (2020). Comparative Study of the Kinetics of Biogas Yield from the Co-digestion of Poultry Droppings with Waterleaf and Poultry Droppings with Elephant Grass. Engineering Sciences, 15(3), 139-150.

Fan J., Shah L., and Furbo S., (2007). Flow distribution in a solar collector panel with horizontally inclined absorber strips, Solar Energy, 81, 1501-1511.

Farahat, S., Sarhaddi, F. and Ajam, H., (2009). Exegetic optimization of flat plate solar collectors. Renewable Energy, 34(3), 1169-1174.

Farghali, M., Osman, A.I., Mohamed, I.M., Chen, Z., Chen, L., Ihara, I. and Rooney, D.W., (2023). Strategies to save energy in the context of the energy crisis: a review. Environmental Chemistry Letters, 1-37.

Gond, B.K., Mittal, S., Prajapati, P. and Khare, R., (2016). Analysis of solar flat plate collector. International journal of research and scientific innovation, 3(7), 105-110.

Hayashi, D., Huenteler, J.T. and Lewis, J.I., (2018). Gone with the wind: A learning curve analysis of China's wind power industry. Energy Policy.

Ikpe, A.E., Ekanem, K.R. and Etuk, E.M., (2021). Simulation of Internal Pipe Flows in Gasoline Port Fuel Injection System Under Steady State Condition. Usak University Journal of Engineering Sciences, 4(2), 79-93.

Ikpe, A.E., Imonitie, D.I. and Ndon, A. E., (2019). Investigation of Biogas Energy Derivation from Anaerobic Digestion of Different Local Food Wastes in Nigeria. Academic Platform Journal of Engineering and Science, 7(2), 332-340.

Ikpe, A.E., Owunna I. and Satope, P., (2018). Simulation of Two Phase Flow Dynamics in Flexible Riser Exit Geometries for Oil and Gas Applications. International Journal of Engineering Research in Africa, 39, 1-13.

Islam. S., Dincer. I. and Yalbas, B.S., (2015). Energetic and exegetic performance analysis of a solar energy-based integrated system for multi generation including thermoelectric generators. Energy, 93, 1246-1258.

Jafarkazemi, F. and Ahmadifard, E., (2013). Energetic and exegetic evaluation of flat plate solar collectors. Renewable Energy, 56, 55-63.

Kalogirou, S.A., Karellas, S., Badescu, V. and Braimakis, K., (2016). Exergy analysis on solar thermal systems: A better understanding of their sustainability. Renewable Energy, 85, 1328-1333.

Kebede, D., (2016). Design and analysis of solar thermal system for hot water supply to Minik II Hospital new building. Addis Ababa University, Ethiopia, 2016.

Klein, S.A., (1977). Calculation of monthly average insolation on tilted surfaces, solar energy laboratory, University of Wisconsin-Madison, Madison, WI 53706, USA.

Kumar, P.M., Sudarvizhi, D., Prakash, K.B., Anupradeepa, A.M., Raj, S.B., Shanmathi, S. and Surya, S., (2021). Investigating a single slope solar still with a nano-phase change material. Materials Today: Proceedings, 45, 7922-7925.

Kurri R.M., (2018). Transient operation and simulation of a flat plate solar collector with tank and thermal storage. Purdue University, Fort Wayne, Indiana, 2018.

Liu, G., Zhou, B. and Liao, S., (2018). Inverting methods for thermal reservoir evaluation of enhanced geothermal system. Renewable and Sustainable Energy Reviews, 82, 471-476.

Markovska, N., Duić, N., Mathiesen, B.V., Guzović, Z., Piacentino, A., Schlör, H. and Lund, H., (2016). Addressing the main challenges of energy security in the twenty-first century–contributions of the conferences on sustainable development of energy, water and environment systems. Energy, 115, 1504-1512.

Muhammad, F.H., Mahadi, S.R., Miyazaki, T., Koyama, S. and Thu, K., (2018). Exergy analysis of serpentine thermosyphon solar water heater. Applied science, 8, 1-17.

NCEE National Centre for Energy and Environment (2017). Climate Data. Energy Commission of Nigeria, University of Benin, Edo State Nigeria.

Omo-Oghogho, E. and Ikpe, A.E., (2020). Angular Solar Relations Analysis of a Flat Plate Solar Collector in Benin City Metropolis. International Journal of Engineering and Innovative Research, 2(2), 67-77.

Omo-Oghogho, E., Ikpe, A.E. and Adeiza, A.S., (2021). Computation of Heat Transfer in a Flat Plate Solar Collector System Using Energy Balance Method. Journal of Energy Technology and Environment, 3(4), 53-61.

Omo-Oghogho, E., Ikpe, A.E., Kwasi-Effah, C. and. Sadjere, E.G., (2021). Empirical Modelling and Estimation of Solar Radiation from Tilted Surfaces Relative to Angular Solar Relations. Journal of Energy Technology and Environment, 3(4), 62-68.

Oselen, I.J., Oseiga, O.V. and Ikpe, A.E., (2019). Design and Performance Testing of a Solar Water Heater. International Journal of Advances in Scientific Research and Engineering, 5(11), 15-22.

Owunna, I.B, Ikpe, A.E., Satope, P.O. and Sangotayo, E.O., (2018). A Preliminary Investigation of Solar Powered Vaccine Refrigerator for Use in Rural Hospitals In Nigeria. University of Benin Journal of Science and Technology, 6, 31-43.

Riaz, H., Ali, M., Akhtar, J., Muhammad, R. and Kaleem, M., (2022). Comparative optical and thermal analysis of compound parabolic solar collector with fixed and variable concentration ratio. Engineering Proceedings, 12(1), 85.

Robert, F., Ghassemi, M. and Cota, A., (2010). Solar energy: renewable energy and the environment. Boca Raton: CRC press.

Saleh A.M., (2012). Modelling of Flat-Plate Solar Collector Operation in Transient States. Purdue University, Fort Wayne, Indiana, 2012.

Singh P., Sarviya R., and Bhagoria J., (2010). Heat loss study of trapezoidal cavity absorbers for

linear solar concentrating collector, Energy Convergence and Management, 51, 329-337.

Vengadesan, E. and Senthil, R., (2020). A review on recent development of thermal performance enhancement methods of flat plate solar water heater. Solar Energy, 206, 935-961.

Yogi, G.D., Kreith, F. and Kreider, J.F., (1999). Principles of solar engineering. 2nd. Philadelphia: Taylor and Francis.

Zhou, J., Ke, H. and Deng, X. (2018). Experimental and CFD investigation on temperature distribution of a serpentine tube type photovoltaic/thermal collector. Solar Energy, 174, 735-742.

Zhou, J., Zhe, Z., Liu, H. and Yi, Q., (2017). Temperature distribution and back sheet role of polycrystalline silicon photovoltaic modules. Applied Thermal Engineering, 111, 1296-1303.